Topochemical conversion of a dense metal-organic framework from a crystalline insulator to an amorphous semiconductor

S. Tominaka,[a,b*] H. Hamoudi,[b] T. Suga,[c] T. D. Bennett,[a] A. B. Cairns[d] and A. K. Cheetham[a*]

[a] *Department of Materials Science and Metallurgy, University of Cambridge, Charles Babbage Road, Cambridge CB3 0FS, United Kingdom. Fax: +44 1223 334567; Tel: +44 (0)1223 767061; E-mail: akc30@cam.ac.uk.*

[b] *International Center for Materials Nanoarchitectonics (WPI-MANA), National Institute for Materials Science (NIMS), 1-1 Namiki, Ibaraki 305-0044, Japan. Tel: +81 (0)29 860 4594; E-mail: TOMINAKA.Satoshi@nims.go.jp*

[c] *Waseda Institute for Advanced Study (WIAS), Waseda University, 3-4-1 Okubo, Shinjuku, Tokyo 169-8555, Japan.*

[d] *Department of Chemistry, University of Oxford, Inorganic Chemistry Laboratory, South Parks Road, Oxford, OX1 3QR, United Kingdom.*

Contents

1. Powder X-ray diffraction data of 1

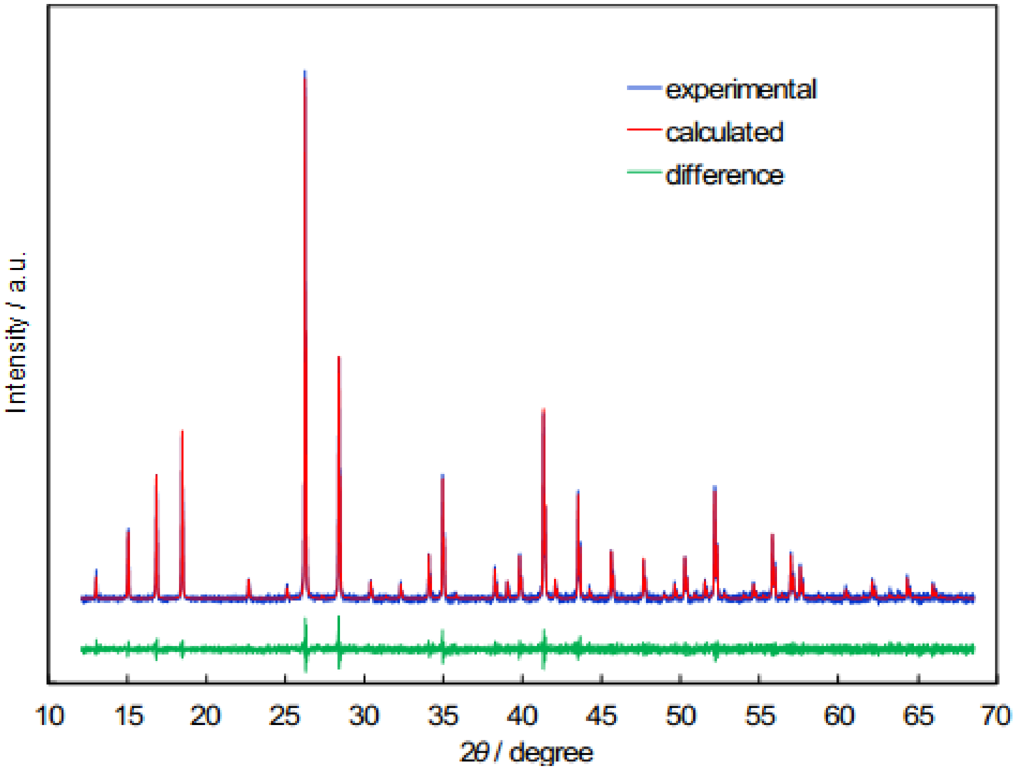

Figure S1 PXRD data of **1** with the Pawley fitting curve.

2. Total scattering patterns obtained using Ag Kα radiation

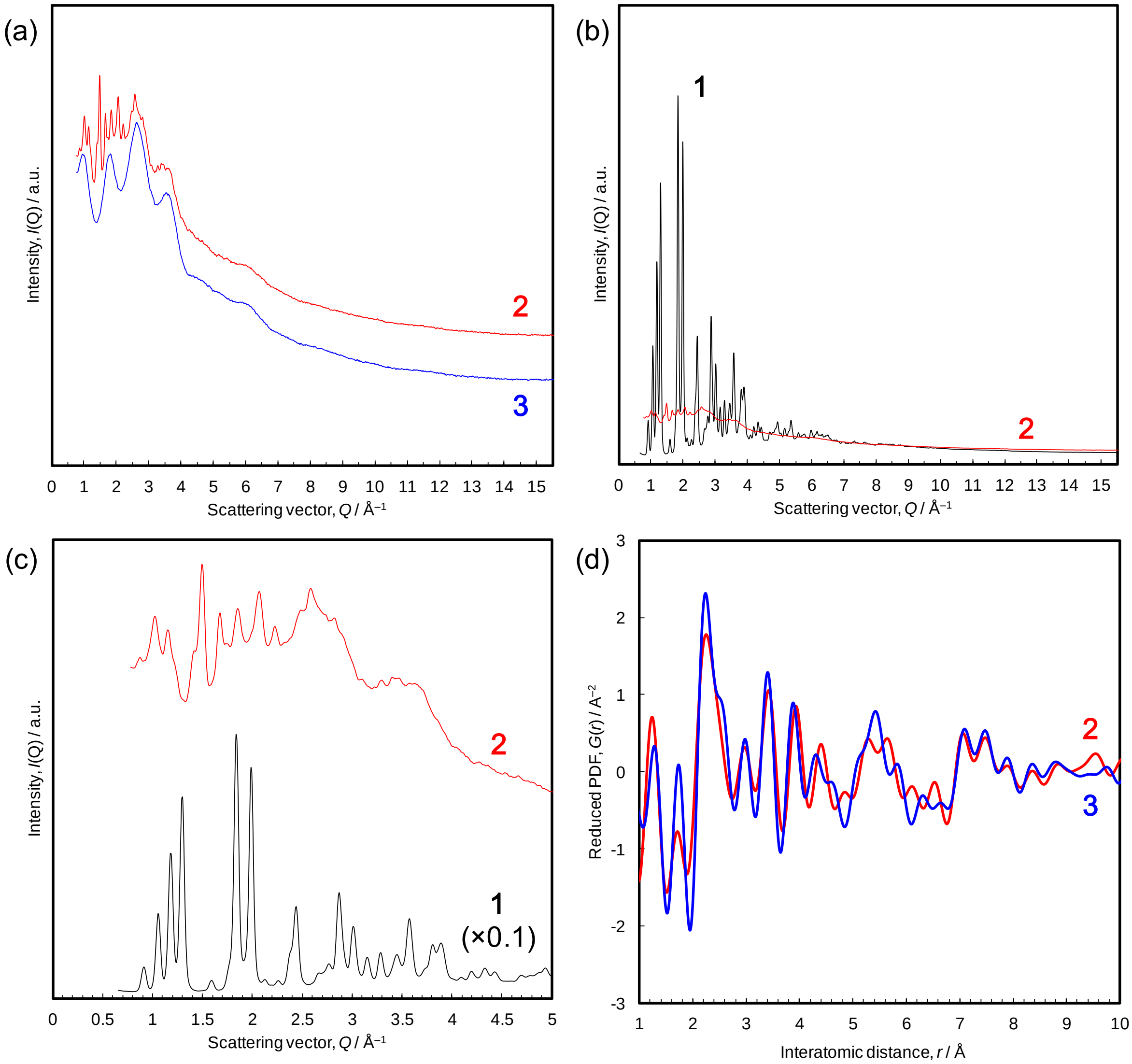

Figure S2 (a-c) X-ray total scattering patterns of compound **1** (black), compound **2** (red) and compound **3** (blue). These data were collected using Ag Kα radiation. (d) Pair distribution functions ($Q_{\max} = 15.5$ Å^{-1}).

3. Thermogravimetric analysis

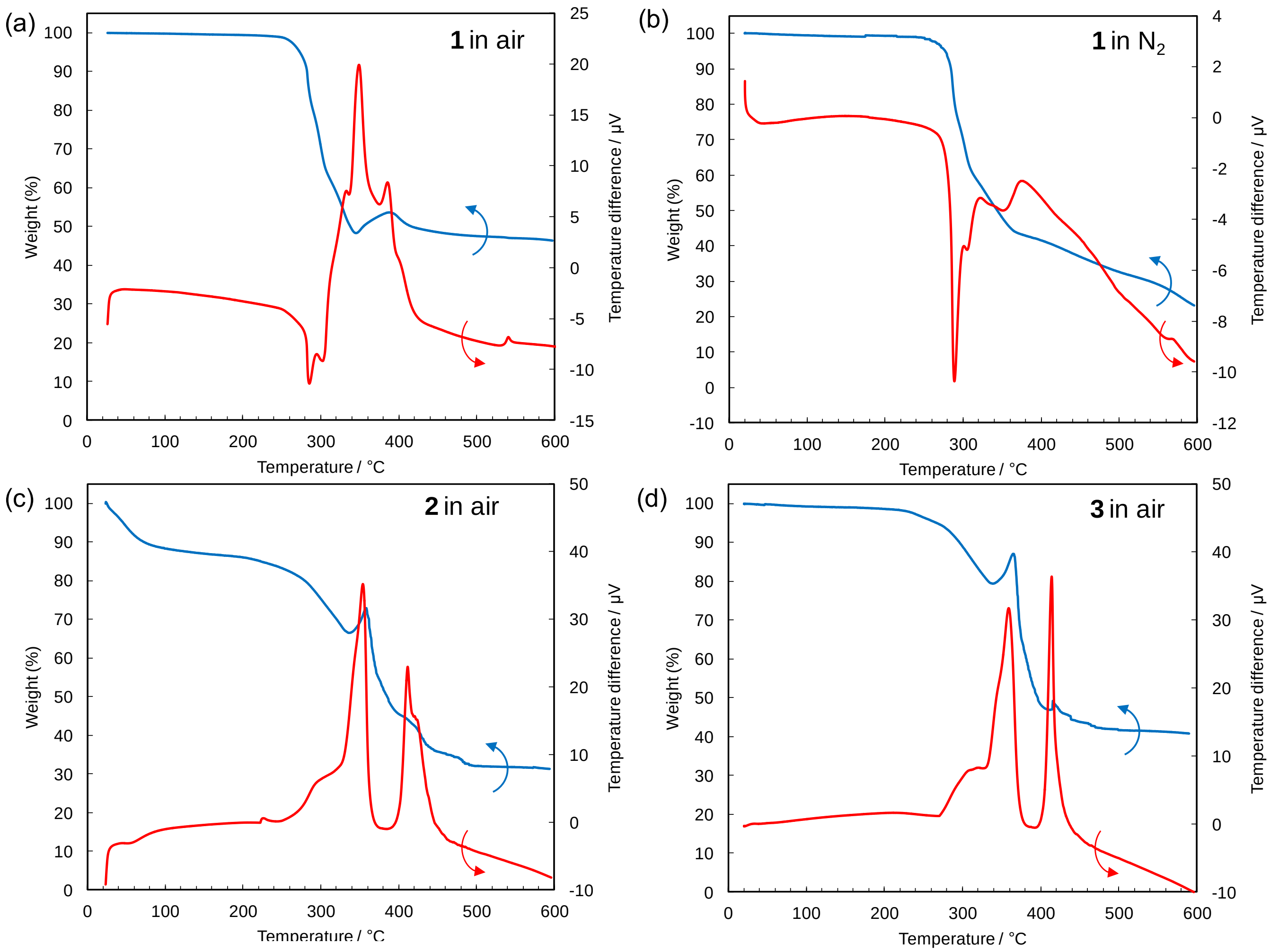

Figure S3 Simultaneous differential scanning calorimetry (DSC)-thermogravimetric analysis (TGA) recorded with air or N_2 flow of 100 mL min^{-1} at scan rate of 5 °C min^{-1}. (a, b) Compound **1**. (c) Compound **2**. (d) Compound **3**.

4. Additional AC impedance data

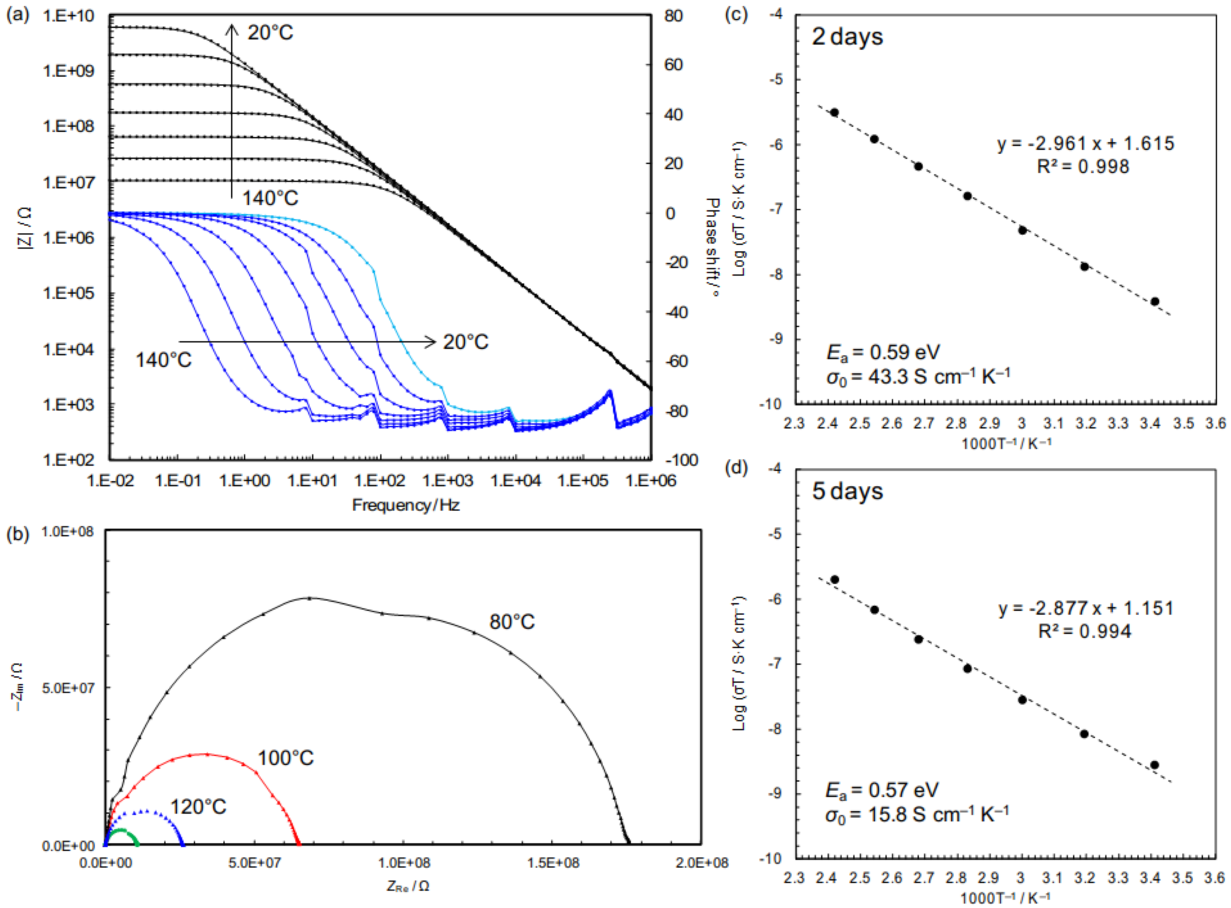

Figure S4 Powder impedance data (Bode plots) of **3**. (a) Bode plots. (b) Complex-plane impedance spectra. (c, d) Arrhenius plots of samples treated for 2 days and 5 days.

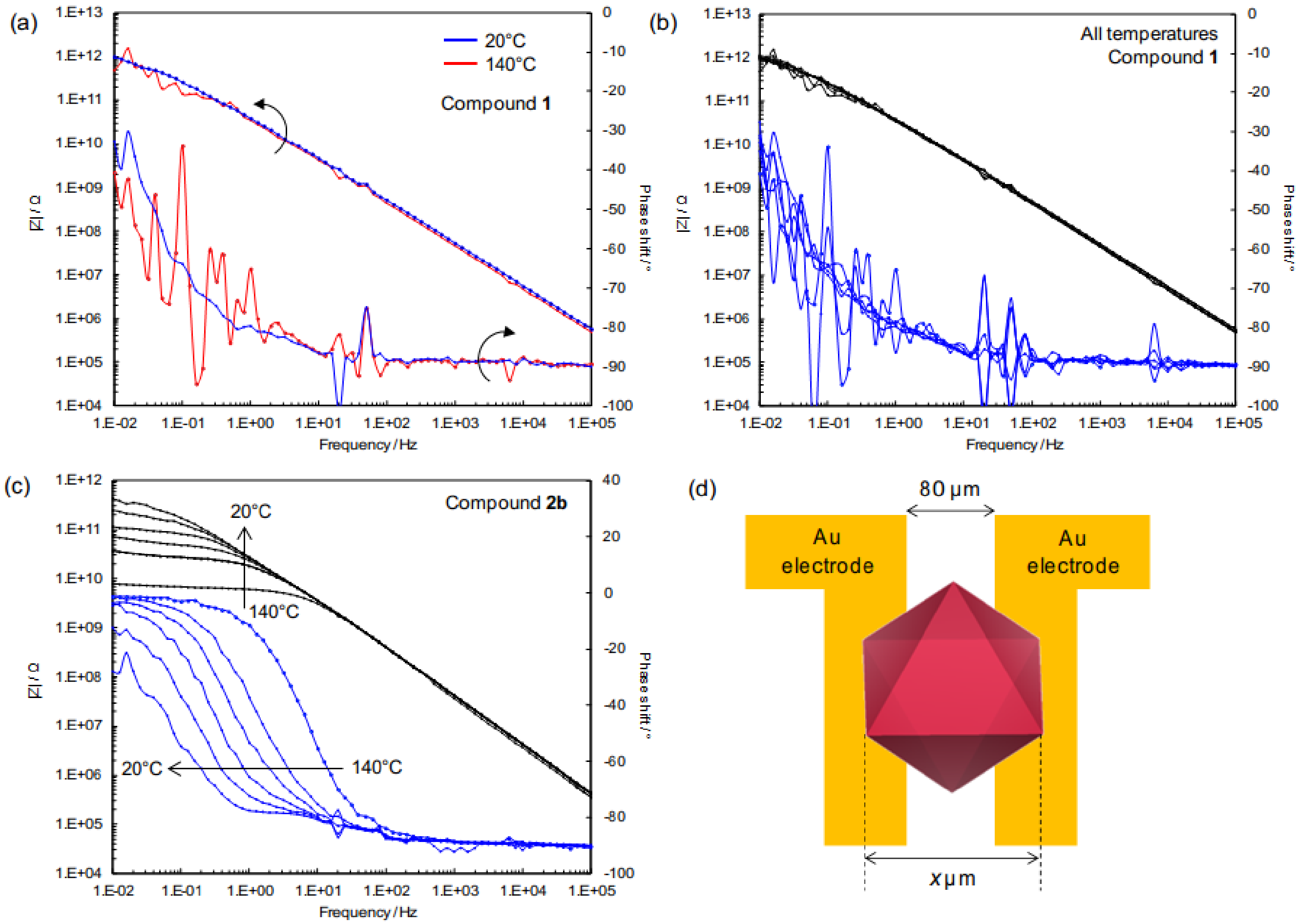

Figure S5 Single-crystal impedance data (Bode plots) of **1** (a, b) and **3** (c). (d) Schematic for illustrating an octahedral crystal placed on microelectrodes. *x* is the length of an edge of octahedron (*x* = 160 µm for **1** and *x* = 130 µm for **3**). Since the shapes and the contact areas of crystals result in non-uniform current density, these measurements are only for distinguishing whether the materials are conductors or not. The size of crystal is roughly 100 µm, meaning the conductivity of **3** is ca. 1 × 10^{-8} S cm^{-1} at 140°C.

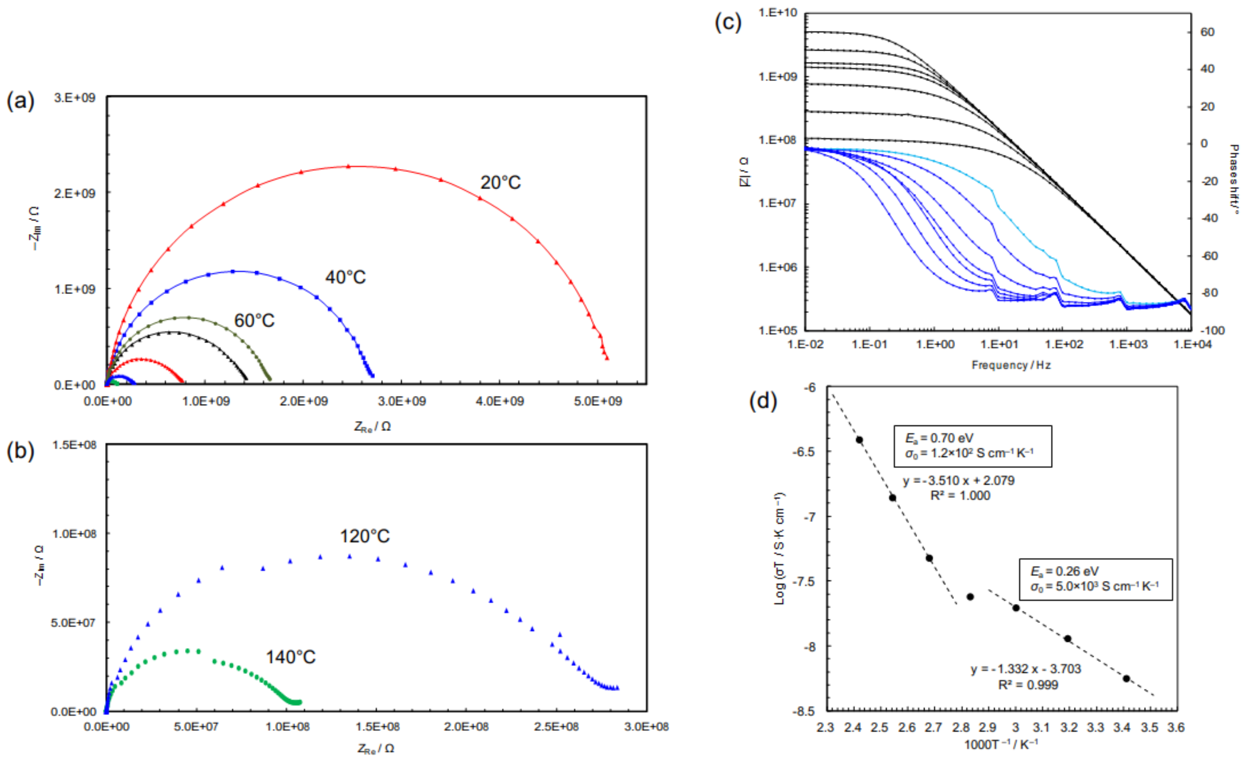

Figure S6 Powder impedance data (Bode plots) of **1**. (a, b) Complex plane impedance plots. (c) Bode plots. (d) Arrhenius plots.

The powder sample of **1** shows semicircular behaviour having a tail at the low frequency region, meaning **1** in a pellet form is an ion conductor. This ionic conductivity is probably due to the defects of Cl^- ions created by the pellet formation.

5. Analysis of temperature-dependent conductivity

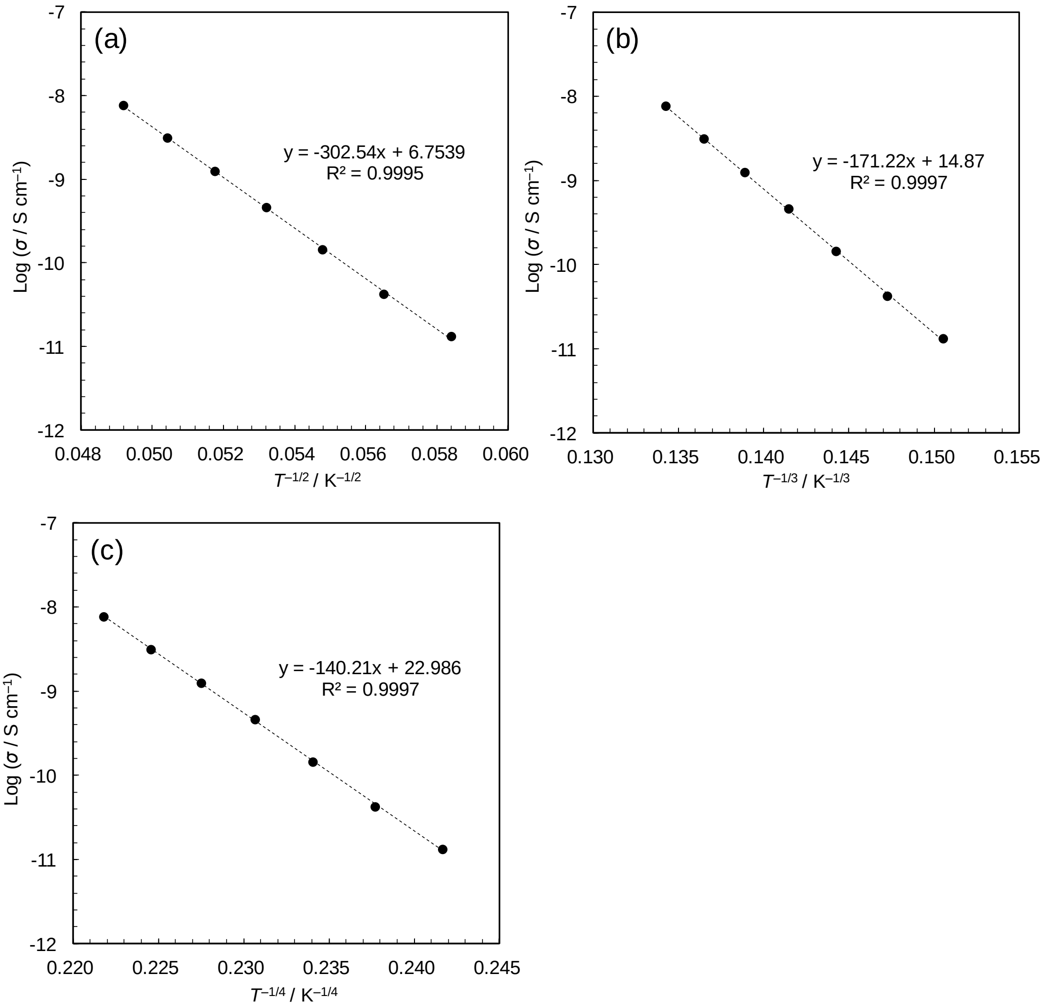

Figure S7 Analysis of conductivity mechanism on the basis of the variable range hopping model: temperature-dependent conductivity plots based on (a) one-dimensional, (b) two-dimension, and (c) three-dimensional conductive pathway.

6. FTIR spectra of the samples treated in a different time

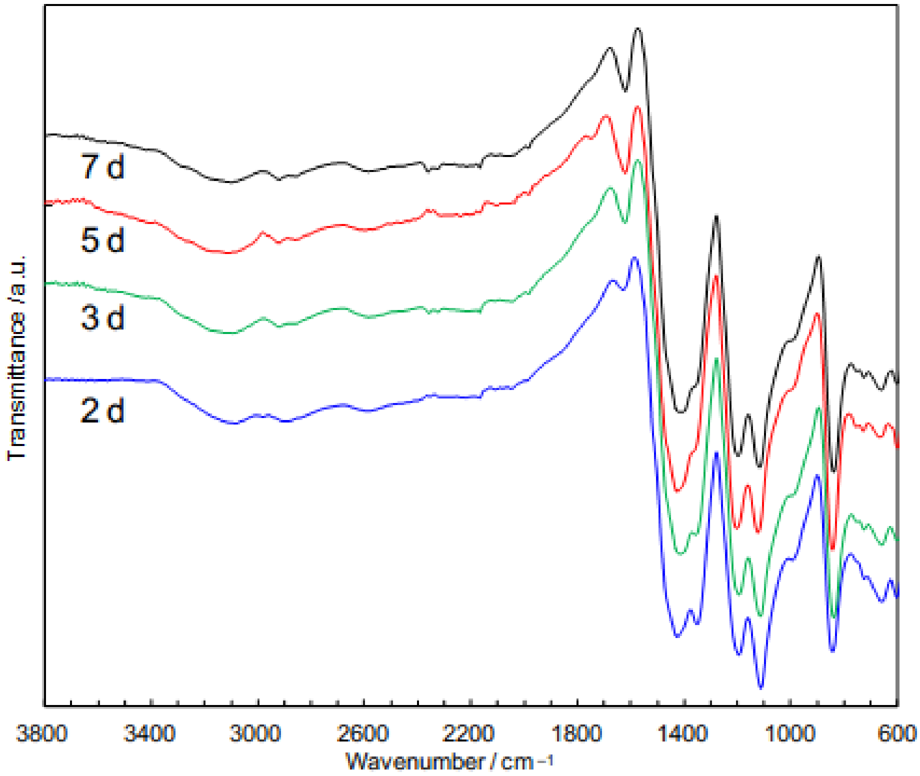

Figure S8 FTIR spectra for comparing the samples treated in a different time. All samples were dried under vacuum; for 2 days, 3 days, 5 days, and 7 days.

7. Cl 2p XPS

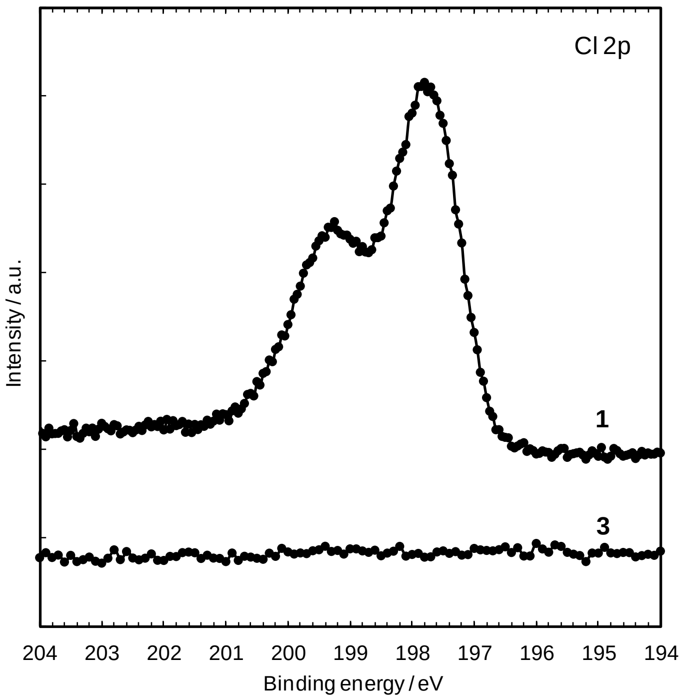

Figure S9 Cl 2*p* XPS of **1** and **3**.

8. PDF analysis

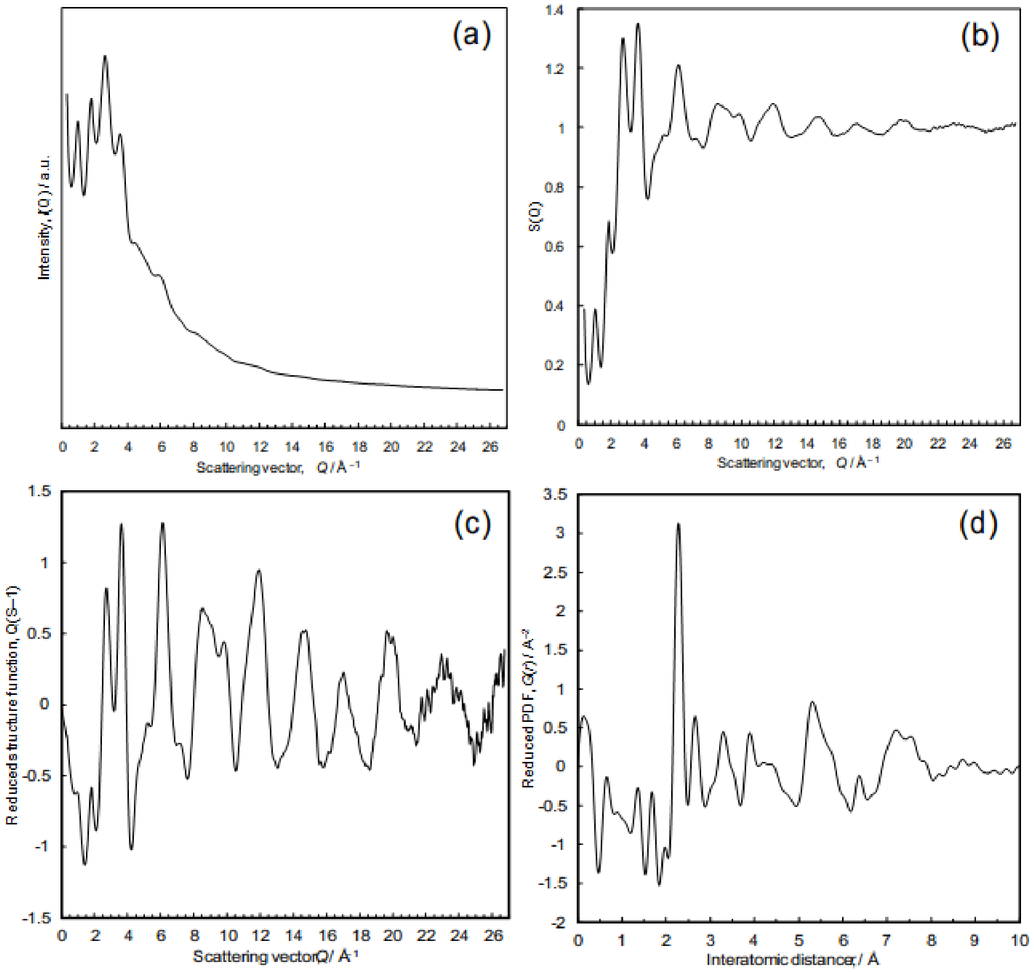

Figure S10 PDF data of **3**. (a) X-ray total scattering pattern with the container scattering correction. This pattern was collected using synchrotron radiation (λ = 0.17220 Å) on the I15 beamline at Diamond Light Source. (b) Structure function, S(Q), vs scattering vector, Q. (c) Reduced structure function, Q(S–1), vs Q. (d) PDF pattern.

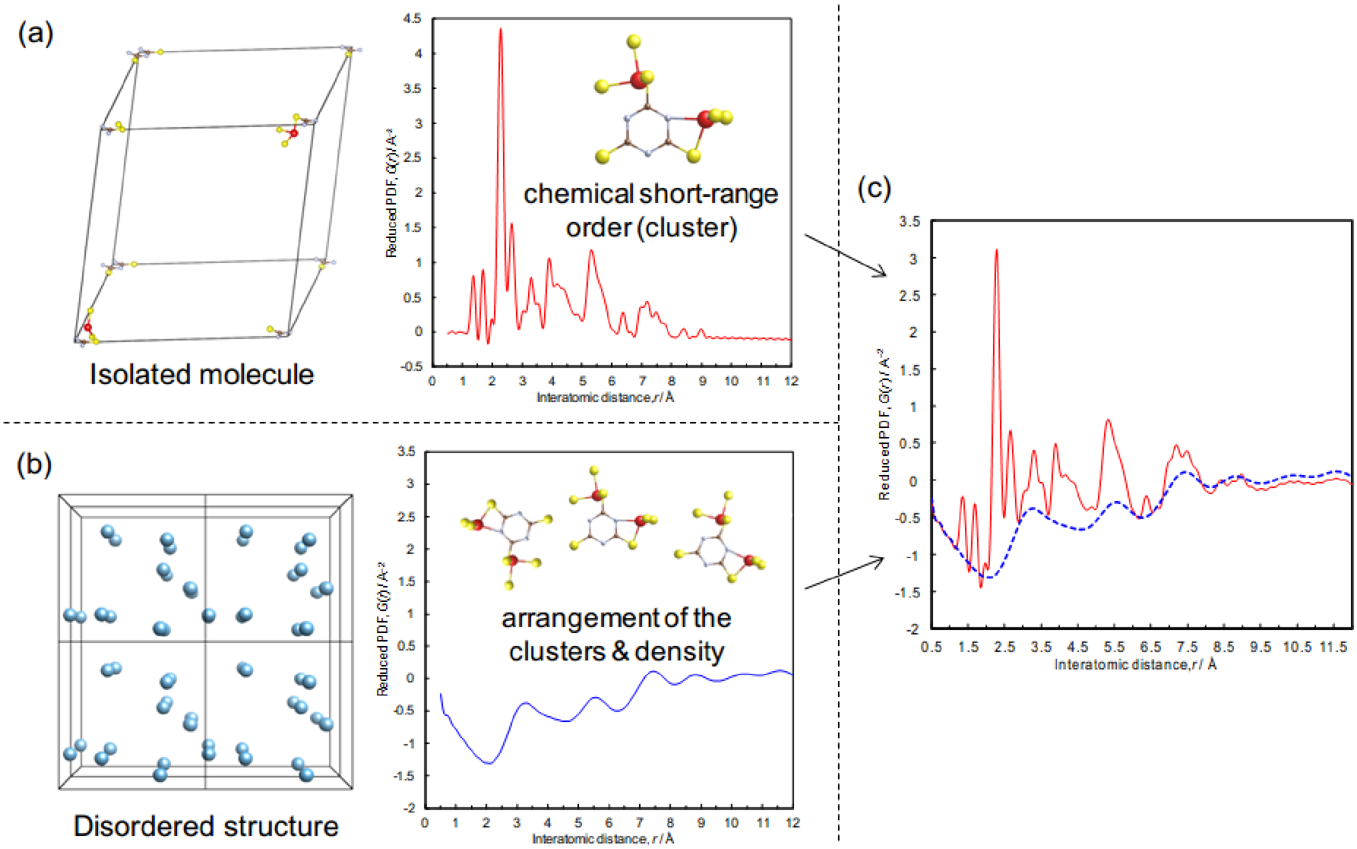

Figure S11 Model for the PDF data analysis of compound 3. (a) Isolated molecule for simulating the chemical short-range order observed as sharp peaks in the experimentally obtained PDF pattern. (b) Arrangement of coordination spheres for simulating the broad oscillation observed in the experimentally obtained PDF pattern. (c) Convoluted simulated pattern.

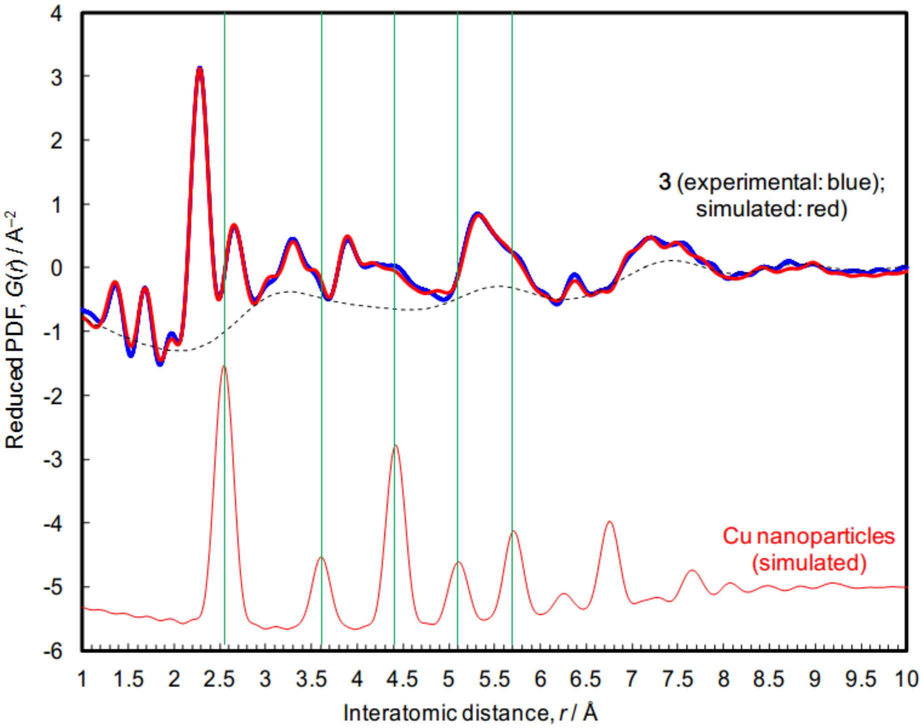

Figure S12 PDFs of **3** and Cu nanoparticles (simulated on the basis of a reported cif file: ICSD 627115, F*m*$\bar{3}$*m*, *a* = 3.61465 Å; and U_{iso} was set to be 0.005 $Å^2$ and the particle size was 10 nm).

9. Samples for single crystal X-ray diffraction

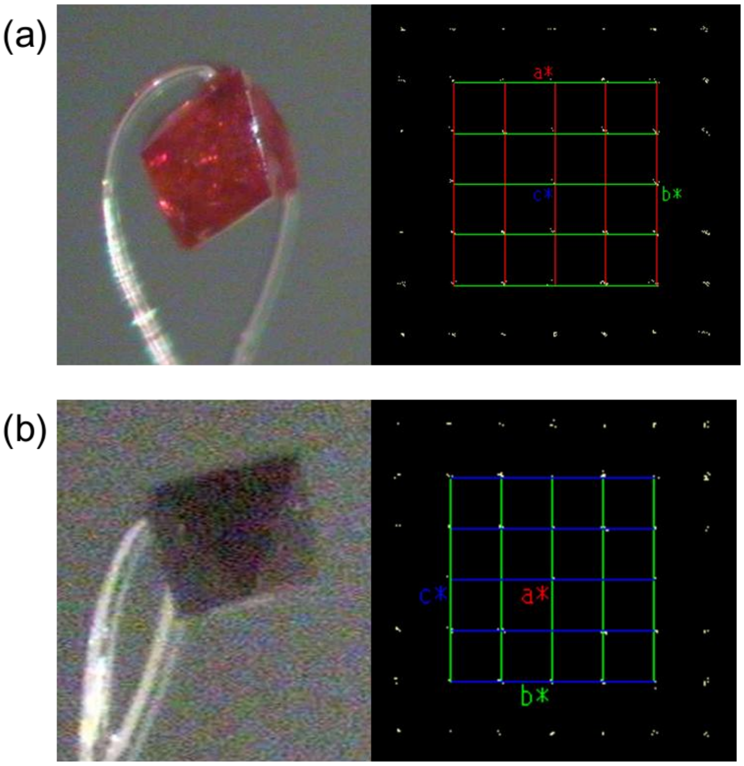

a = 11.70071(13) Å
at 120K

a = 11.6862(3) Å
at 120K

Figure S13 Single crystal X-ray diffraction analyses on **1** (a) and 1 treated in NH_3 aq. solution for <2 days (b). The latter has the same appearance as **2**, but still has diffraction attributable to **1**.

10. DFT calculations

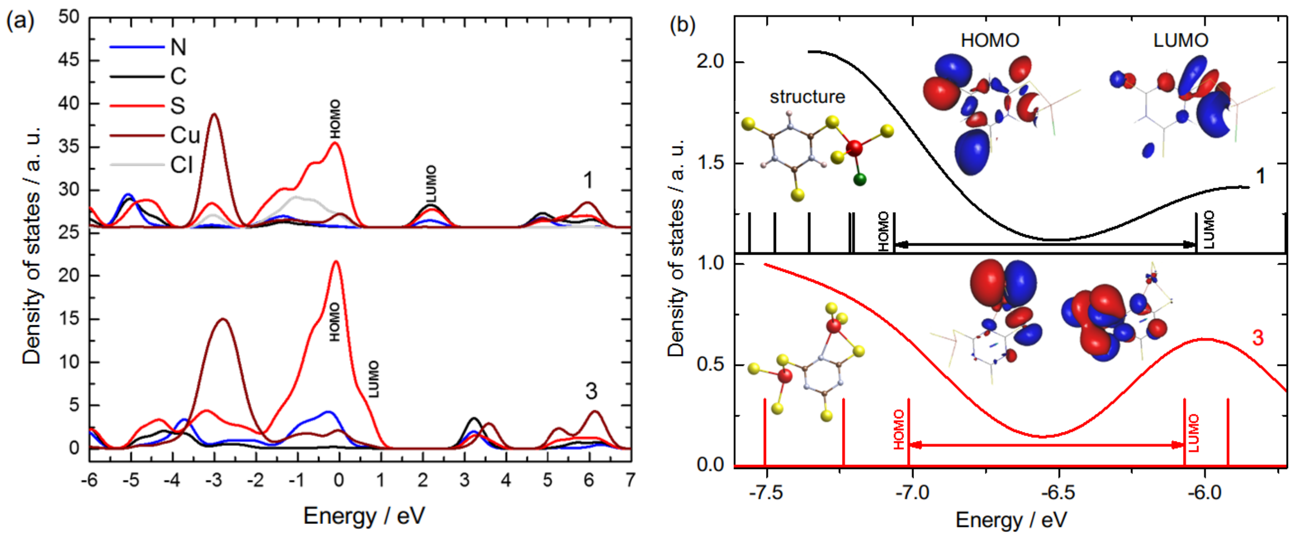

Figure S14 Density of states of frontier orbitals in **1** and **3** obtained by DFT calculations: (a) Plane wave (CASTEP). (b) Isolated molecules (ORCA).

Plane wave calculations: The calculations have been performed using density functional theory (DFT) with ultra-soft pseudopotentials[1] and a 230 eV energy cut-off. A plane wave basis set has been used, and the exchange-correlation has been treated with the generalized gradient approximation (GGA). Adsorption energies and density of states (DOS) were calculated with the CASTEP package[2]. The integration over the surface Brillouin zone is done on a 1 1 1 k-point sampling grid. The slab was repeated periodically with 18 Å of vacuum between the slabs. The Perdew, Burke and Ernzerhof (PBE) exchange-correlation functional [3] was used. In the partial density of states PDOS (Figure S15), the energy, $E = 0$, means the center of the HOMO orbital.

In the calculations, **1** was treated as a crystalline system while **3** was treated as a locally ordered system, which has the representative local structure determined by the PDF refinement. Thus, the former corresponds to the electronic structure of **1**, while the latter represents local electronic structure of **3**. We believe these calculations are useful enough to interpret the experimental data although the calculations, especially of **3**, are preliminary to understand electronic structure of its entire system. In order to double-check the results, we performed additional calculations on isolated molecules as follows.

Figure S15a shows that the C, N, S, Cl and Cu contributions in the partial DOS of the systems **1** and **3**. The HOMO and the LUMO are localized on the sulfur groups in both cases. The HOMO-LUMO band gap is smaller in **3** compared to **1**. The removal of the Cl ions, which have strong bonding with Cu, shifts the Cu *d*–band center up in **3**. This Cu *d*-band in turn shifts the S *p*-band up in **3**, resulting in the formation of unoccupied states just above the Fermi level.

Isolated molecules: Theoretical calculations were performed using the ORCA program[4] for the Cu coordination sphere(s) with a trithiocyanurate molecule of **1** and **3** as shown in Fig. 6. The PBE0 model[5] was used in combination with triple-zeta plus polarization basis set [Ahlrichs TZV (2df, 2pd)].[6] Figure S15b clearly shows that the HOMO–LUMO band gap of **3** is smaller than **1**. In both materials, the HOMO and the LUMO are localized on the sulfur groups.

References:

1. D. Vanderbilt, *Phys. Rev. B.*, 1990, **41**, 7892-7895.
2. M. D. Segall, P. J. D. Lindan, M. J. Probert, C. J. Pickard, P. J. Hasnip, S. J. Clark and M. C. Payne, *J. Phys. Cond. Matt.*, 2002, **14**, 2717-2743.
3. J. P. Perdew, K. Burke and M. Ernzerhof, *Phys. Rev. Lett.*, 1996, **77**, 3865-3868.
4. F. Neese, *Wiley Interdiscip. Rev.: Comput. Mol. Sci.*, 2012, **2**, 73-78.
5. C. Adamo and V. J. Barone, *J. Chem. Phys.*, 1999, **110**, 6158-6170.
6. A. Schäfer, H. Horn and R. Ahlrichs, *J. Chem. Phys.*, 1992, **97**, 2571-2577.
7. C. F. Macrae, I. J. Bruno, J. A. Chisholm, P. R. Edgington, P. McCabe, E. Pidcock, L. Rodriguez-Monge, R. Taylor, J. van de Streek and P. A. Wood, *J. Appl. Cryst.*, 2008, **41**, 466-470.

11. Diffuse reflectance spectra

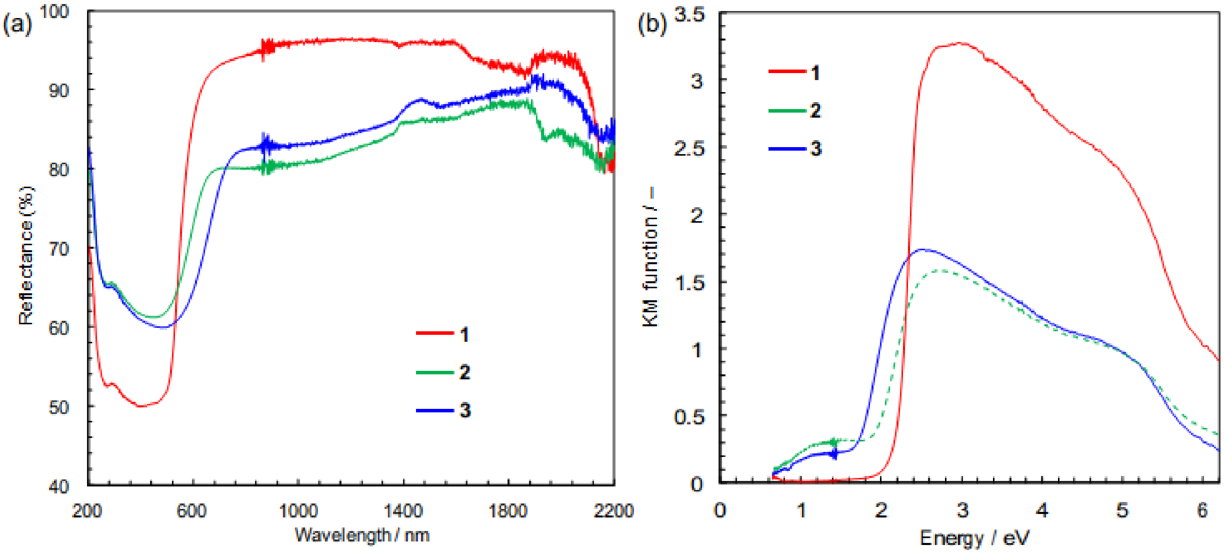

Figure S15 (a) Diffuse reflectance spectra of the samples diluted to be 10 wt% with $BaSO_4$, and (b) Kubelka-Munk functions with concentration corrections.

12. ESR spectra

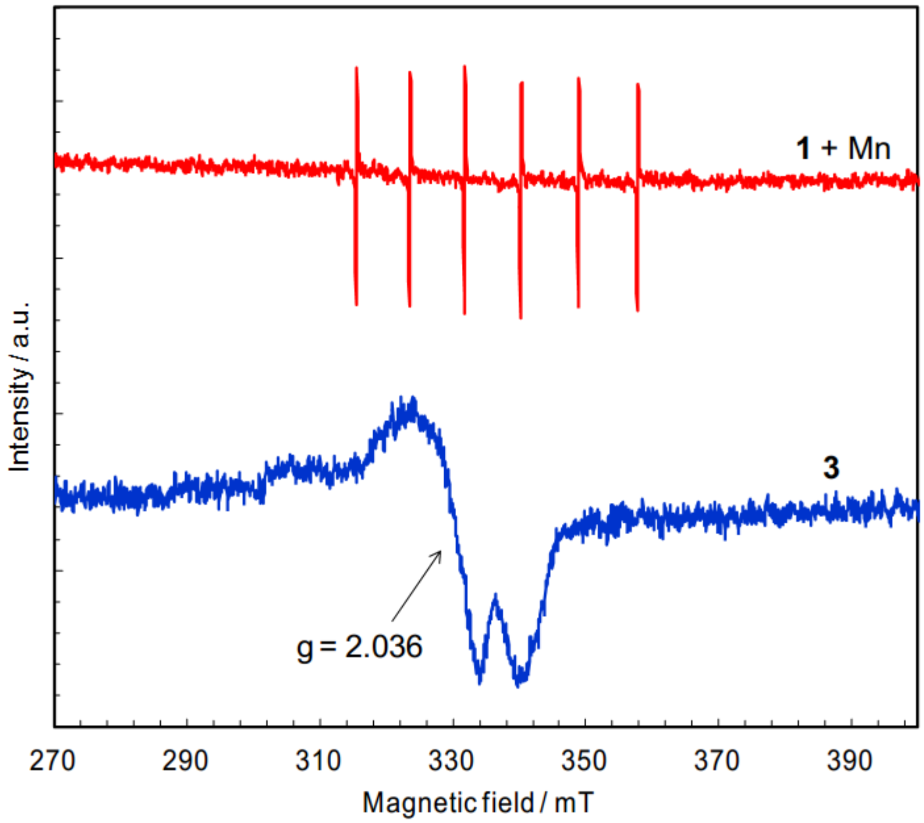

Figure S16 ESR spectra.